# EXPERIMENTAL AND NUMERICAL ANALYSIS OF WATER HAMMER DURING THE FILLING PROCESS OF PIPELINES

Cristiano Bombardieri, Tobias Traudt, Chiara Manfletti
*Engine Transients Group, Institute of Space Propulsion*
*German Aerospace Center (DLR), 74239 Hardthausen, Germany*

**Abstract**

During the start-up of the propulsion system of a spacecraft, the filling of an evacuated pipeline, a process known as priming, can generate severe pressure peaks due to the slam (water hammer) of the propellant against a closed thruster valve. The downstream conditions strongly affect the pressure surge; in the case of evacuated lines these pressure peaks can be as high as 250 bar and may lead to structure failure if not properly taken into account in the sub-system dimensioning. At DLR Lampoldshausen a new test-bench has been built in order to investigate priming process and other fluid transient phenomena.

The experimental investigation presented in this paper includes priming test in both pre-pressurized and evacuated pipelines. Geometry of the test-section is a 2000 mm straight pipe with a relative large diameter (19mm) in order to examine high mass flow .

From a physical point of view, the modeling of priming is a complex task, as it involves transient multiphase flow. As a first approach, an analytical model of the equations of motion is solved by applying the rigid liquid column theory, considering only the inertial and frictional effects of the liquid treated as a slug. The friction plays an important roles, in particular due to the unsteady conditions which increase its steady value. The cushion effect of an inert gas is also analyzed and the assumption of adiabatic vs isothermal compression compared. Results indicated that a polytropic compression can better model the realistic gas behavior.

Finally, using a EcosimPro® numerical model of the test-bench (in conjunction with the ESPSS library, an ESA-developed tool capable of one dimensional, two-phase flow transient simulations), a comparison between numerical results against experimental data is presented and discussed.

Keywords*: water hammer, fluid transient, priming, EcosimPro ESPSS*

## NOMENCLATURE

| | |
|---|---|
| $\rho$ | density [Kg/m^3] |
| $\dot{m}$ | mass flow [Kg/s] |
| P | pressure [bar] |
| $P_t$ | tank pressure [bar] |
| $P_g$ | gas pressure [bar] |
| $L_{up}$ | upstream pipe length [m] |
| $L_d$ | downstream pipe length [m] |
| ID/OD | internal/outer diameter [m] |
| V | flow velocity [m/s] |
| $K_v$ | valve pressure loss coefficient [-] |
| $\lambda$ | friction coefficient [-] |
| $\gamma$ | specific heat ratio [-] |
| c | speed of sound [m/s] |
| T | temperature [K] |
| FOV | fast opening valve |

Corresponding author:
cristiano.bombardieri@dlr.de

## 1 INTRODUCTION

During the start-up of the propulsion system of a spacecraft, the filling of an evacuated pipeline, a process known as priming, can generate severe pressure peaks due to the slam (water hammer) of the propellant against a closed thruster valve. For safety reasons, the propellant feedlines of a satellite or spacecraft engine are evacuated or filled with a small amount of inert gas prior to the launch.

Once in orbit, the tank isolation valve opens (usually a pyrotechnic valve) and the evacuated lines are filled with the propellant. When the liquid propellant impacts the closed thruster valve or other dead-ends, it can create pressure peaks as high as 250 bar that may lead to structural failure if not properly taken into account in the pipeline and sub-system dimensioning. In the case of hydrazine or a mono-propellant in general, another potential risk must be considered: the rapid compression of inert gas or propellant vapor generates heat and may cause adiabatic compression detonation. A pressure surge in hydrazine cannot exceed 172 bar (2500 psi) due to the risk of adiabatic det-

onation [1].

To prevent these two potential hazards, the solution is to slow down the flow through the use of either a flow restriction device (venturi [2] [3] or orifice [4][1]) or the gas cushion effect. However, the addition of flow restriction devices increases the system pressure loss.

For some missions, a small amount of gaseous helium is loaded into the propulsion subsystem downstream of the closed latch valves. It acts as a cushion to the liquid front and proves to be an effective way to decrease the surge pressure [2].

Gibec and Maisonneuve [5] performed water hammer experiments with real propellants, namely MMH, NTO and hydrazine, for different pipe geometries including straight, bend, elbow and tee pipes. They hypothesized that phenomena such as cavitation, pipe deformation and vapor pressure may interfere with the water hammer.

Lema et al.[6] investigated the effect of a fully saturated liquid compared to the deareated one in vacuum conditions. Test results showed that for the saturated liquid the pressure peak is slightly smaller due to the desorption of the dissolved gas which acts as a cushion in front of the liquid. Flow visualization with high speed imaging was also conducted by means of a quartz pipe at the dead-end, which provides a remarkable insight of the multi-phase fluid hammer process.

Lecourt and Steelant [7] performed several test with ethanol, acetaldehyde and MMH for straight and bend pipes. They observed a surprising multiple steps evolution of the first pressure peak. They also demonstrated that ethanol can be used as a replacement fluid instead of toxic MMH.

This paper presents both an analysis of the priming process based on the liquid column theory and the test results obtained from experiments in evacuated and pre-pressurized lines.

# 2 ANALYSIS OF MOTION

To analyze the priming process, the liquid column theory is applied as a first approach. It considers the propellant in the feedlines as an incompressible liquid slug and analyzes its unsteady motion. The analytical model based on the rigid liquid column theory has been applied to the priming process of a satellite propulsion system in many studies [8][9][10][2].

An analysis of motion applied to pipe filling case was first proposed by Yaggy [8]. In his work the parameters investigated are tank pressure, upstream and downstream line length, propellant (NTO and MMH) and friction factor. The assumptions for the model are the same as for all the following studies that used the rigid liquid column theory, including the present analysis, and are therefore here summarized:

1. fluid can be treated as a slug flowing into the line
2. gas solubility is negligible: the amount of pressurant gas in the line prior to valve opening remains constant during compression
3. vaporization of propellant produces a negligible amount of gaseous propellant
4. due to high shock speeds in the pressurant gas, the gas is everywhere at the same pressure
5. system conditions are constant over time
6. gas behaves adiabatically
7. the propellant lines are assumed to be infinitely rigid

Prickett et al. [9] employed an analogous model for the calculation of peak surge pressures. An application of the analysis indicates the beneficial effects of pre-pressurization of the downstream lines with gas in order to reduce the peak pressure surge. Compared to the experimental data, the numerical predictions gives satisfactory results.

Lin and Baker [10] used the method of characteristics to treat one-dimensional liquid transients in liquid-full segments, and the lumped-inertia technique to model the dynamics of partially filled (or two-phase) segments. Fluid compressibility and piping flexibility are also taken into account.

Hearn [2] developed a methodology for analytical prediction of priming surge pressures based as well on the rigid liquid column approach. In his work, he analyzed complex geometries and underlined the importance of fluid branching and manifold volumes, since they are used in the determination of the order in which different regions fill. The technique has been validated against actual measurements of water hammer pressures and provides acceptable accuracy in many cases.

## 2.1 Equations of motion

The assumptions for the analytical model are the same as discussed above. The fluid is modeled as a rigid column accelerating upon valve opening and including both inertia and friction effects.

The equations of motion for the slug are then obtained from the Newton's second law $F = m\ddot{x}$ . The force acting on the liquid are the pressure difference (positive) and the friction.

Referring to Fig.1, $L_{up}$ and $L_d$ are the upstream and downstream length respectively, $P_t$ the tank pressure, $P_{v,up}$ and $P_{v,d}$ the pressure across the valve, $A$ the pipe cross section, $\rho$ the fluid density, $\lambda$ the friction.

The force balance can be written as:

$$\rho L_{up} A\ddot{x} = (P_t - P_{v,up})A - \frac{1}{2}\rho\dot{x}^2\frac{L_{up}}{D}\lambda A \qquad (1)$$

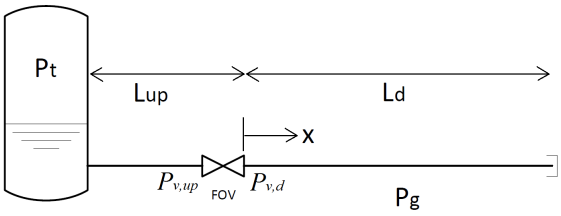


Figure 1: Fluid system model

where $x$ is the fluid position variable.
The same applies downstream of the valve:

$$\rho x A \ddot{x} = (P_{v,d} - P_g)A - \frac{1}{2}\rho \dot{x}^2 \frac{x}{D}\lambda A \tag{2}$$

The equation for the flow through the valve is

$$P_{v,up} - P_{v,d} = \frac{1}{2}\rho \dot{x}^2 K_v \tag{3}$$

where $K_v$ is the valve pressure loss coefficient.
The upstream pressure $P_{v,up}$ is the tank pressure (total pressure) minus the dynamic pressure to take into account the transformation of kinetic energy and the tank inlet pressure loss $K_{inlet}$

$$P_t = P_{v,up} + \frac{1}{2}\rho \dot{x}^2 (1 + K_{inlet}) \tag{4}$$

The gas behavior downstream can be treated as adiabatic compression ($\gamma = 1.4$):

$$P_g = P_{g0}\left(\frac{L_d}{L_d - x}\right)^{\gamma} \tag{5}$$

Combining the previous relationships, the final equation is a second order non-linear differential equation:

$$\rho(L_0 + x)\ddot{x} = \tag{6}$$
$$= (P_t - P_{g0}\left(\frac{L_d}{L_d - x}\right)^{\gamma}) - \frac{1}{2}\rho \dot{x}^2 \left(\frac{L_0 + x}{D}\lambda + 1 + K_v + K_{inlet}\right)$$

Equation 6 is solved by forward finite difference method, obtaining distance $x$, velocity $\dot{x}$ and acceleration $\ddot{x}$ versus time.

For the evacuated downstream pipe case, the water-hammer pressure peak is calculated based on the final velocity $V_f$

$$P_{wh} = \rho c V_f$$

being $c$ the speed of sound. Important to mention, the speed of sound is affected by the gas content in the liquid (pressurant gas dissolved in the liquid).

In the case of pre-pressurized line, being the impact velocity zero, the water hammer pressure is the compressed gas pressure $P_{wh} = P_g(end)$.

Results of the analysis applied to the present test conditions are presented later in Section 4.3 with a comparison against experimental data.

### Friction factor

The pressure peak has been found to be very sensitive of the friction factor value, a conclusion already drawn in previous works [8][9][10][2]; therefore some special attention is required for an educated choice of $\lambda$. The friction factor is determined from the usual Moody diagram using the instant value of the velocity (updated at each iteration). Other choices are also possible: to speed up the calculations the friction factor can be estimated on the maximum expected velocity [8]; in [9] the friction is set so that the calculated impact time is the same as the experimental data; in [2] a constant conservative value of 0.02 is chosen.

The effect of the friction on the velocity profile for three different cases is shown in Fig. 2.

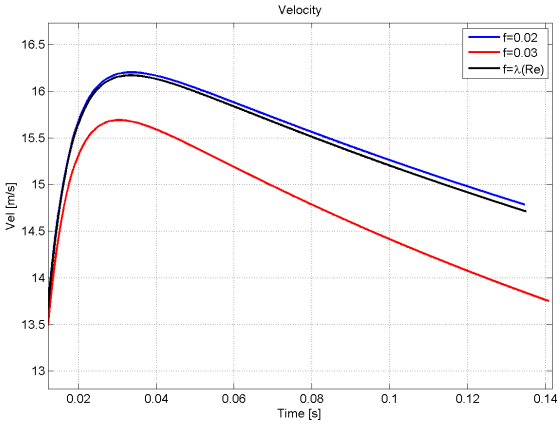


Figure 2: Friction effect on the velocity profile

An important remark is that frictional effects for steady flow and accelerating flow differ. Since the friction coefficient obtained from the Moody diagram is for flows with fully developed viscous boundary layers, the friction coefficient for accelerating flow needs to be modified. This will be further discussed in paragraph 5 for the numerical simulation with EcosimPro.

### Gas compression model

The gas compression process shall be close to the adiabatic process due to the rapid time scale, however, the mixing of water with gas, the possible desorption of the dissolved gas in the water and the heat transfer to the wall will certainly contribute to deviate from the adiabatic process.

In the already mentioned works, the gas behavior is treated as adiabatic. Lin and Baker [10] made also a comparison with the isothermal compression model. In their experiments, the measured pressure peaks fall between the

adiabatic and isothermal predictions, being the adiabatic slightly better in terms of error difference. In the present work, a more general polytropic process ($PV^n = constant$) is considered. The polytropic index $n$ is varied between the two value $\gamma = 1$ (isothermal) and $\gamma = 1.4$ (adiabatic). A parametric study indicates that $\gamma = 1.3$ fits better the experimental results. Comparison between pressure peaks calculated with different polytropic process and experimental results is presented in Section 4.3.

# 3 EXPERIMENTAL SET-UP

## 3.1 Test-bench description

In order to investigate and gain detailed insight into the phenomena of fluid transient such as water hammer (upon valve closing or upon valve opening as investigate in this paper) a new test bench has been built at DLR Lampoldshausen.

The test bench features a 80 liters run tank pressurized up to 50 bar, a flexible pressurization system (GN2 or GHe as a pressurant gas, up to 50 bar) as well as a modular test section with its own conditioning system. This modularity ensures that the test bench is not limited to one test section. Conditioning of the test section can be either done via evacuation or pressurization.

The test bench is equipped with a fast acting valve, pneumatically actuated.

### Fast opening valve

As reported in previous works [6][10][7], the valve opening should be faster than the impact time of the liquid front at the dead-end. In other words, the valve must be fully open before the liquid reaches the end of the test-element pipe. The impact time, as shown later, is in the range 100-150 ms. As a fast opening valve, a co-axial valve is chosen. It is pneumatic actuated (up to 40 bar actuation pressure) and its opening time is only 6 ms. The valve seat is 16mm and its pressure loss coefficient is 12.5. The valve is mounted on a rigid support to limit vibrations during the opening.

The valve opening transient is of importance for numerical validation. It is an important boundary condition although its value not always available. A requirements for the experimental set-up was therefore to have a position measurement sensor to ensure reproducibility of the valve opening transient.

The valve features a position encoder, and its opening profile has been perfectly reproducible over all the performed tests. An example of the position measurement of the valve opening is given in Fig.3.

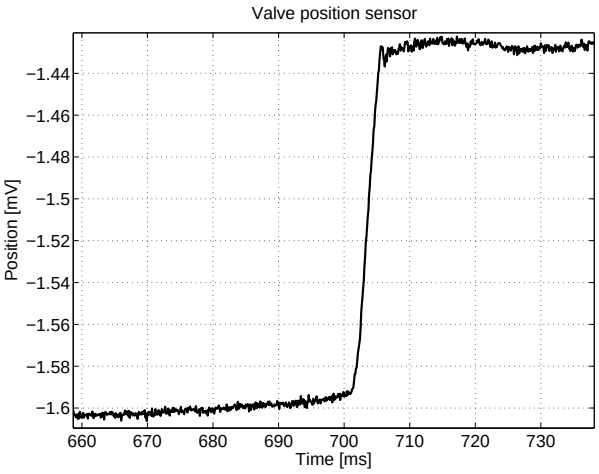


Figure 3: Position measurement of the valve: complete opening is achieved in 6 ms

### Geometry for priming test

Schematic of the test facility is shown in Fig. 4. The geometry of the test-element is a 2000 mm straight stainless steel pipe with a relative large outer diameter (3/4 inch or 19.05 mm) in order to examine high mass flow that are typical of spacecraft feedlines like the ESA automatic transfer vehicle ATV.

The wall thickness of the test section is 1.25 mm (ID 16.56mm) . At five points it is mounted onto a rigid support structure to limit its movements. The support structure is made of aluminium profiles. The test section is mounted with a downward slope of about 1° to facilitate the purging procedure. The upstream part, from the tank to the valve, is a 22x1.5 mm straight stainless steel pipe. For the priming configuration, a tee piece is inserted 350 mm upstream the valve to allow purging and evacuation procedure. Detailed geometry of the test-bench is as follows:

- upstream pipe: OD 22x1.5 mm, stainless steel 1.4541, $L_{up} = 1023mm$
- downstream pipe: OD 19.05x1.44mm, stainless steel 1.4541, $L_d = 2000mm$
- tee piece: OD 22x1.5 mm, stainless steel, at 350 mm upstream of the valve, branch length to MV-2 : 130 mm
- valve seat : 16 mm
- valve pressure loss coefficient $K_v = 12.5$

The same geometry data are also used for the numerical calculations.

Initially a OD 22x1.5mm pipe has been used for the test-element, connected to the valve and to the dead-end by

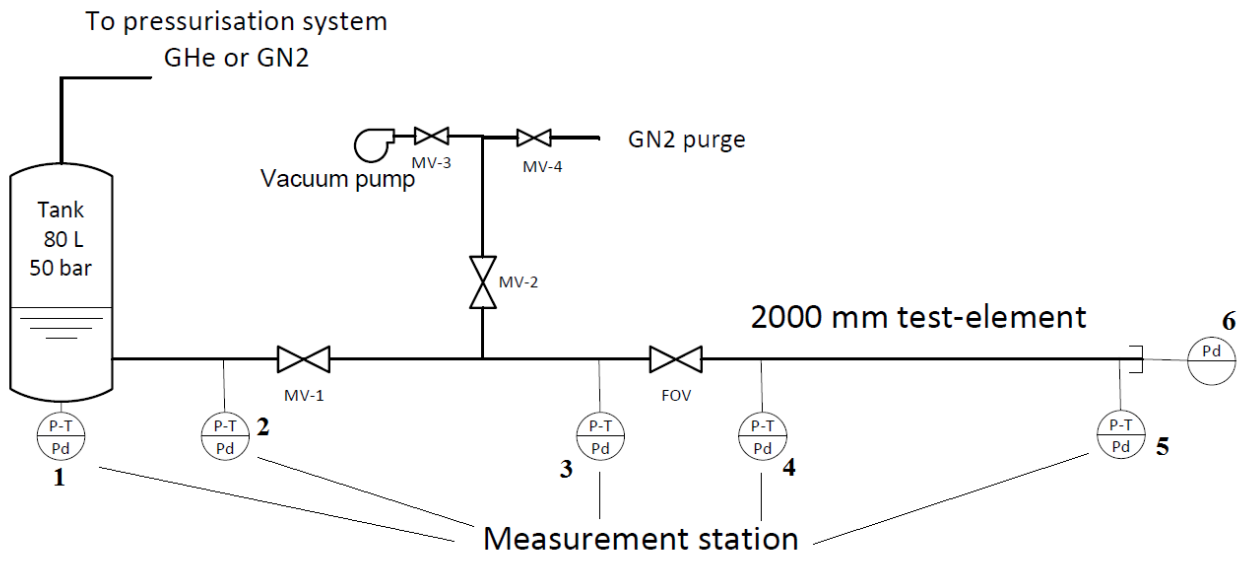


Figure 4: Schematic of M3.5 Fluid Transient Test Facility

means of flanges. Preliminary results, although well reproducible, give a pressure peak lesser than expected. This is likely due to the poor stiffness of the flange connection that is less rigid compared to a welding or screw connection. A more rigorous comparison of the connection effects is in progress. The 19 mm diameter test-section has been connected via a welding upstream and via a screw connection at the end (Fig.5).

**Sensors**

Measurements of pressure and temperature is performed at 6 different stations as shown in Fig.4. Each measurement station consists of 3 transducers: one thermocouple type K, 1 KHz sampling rate; one absolute piezoresistive pressure sensor type 4043A200 from *Kistler*, 10 KHz sampling rate; one dynamic piezoelectric pressure sensor type 601A from *Kistler*, 150 KHz sampling rate.

To avoid aliasing and high-frequency noise, the filter of the dynamic pressure sensors has been set to 30 KHz.

Sensors are screw in a 20 mm thick disk that is mechanically connected by means of a flange (detail shown in Fig. 6). Dynamic pressure sensors (5.5 mm diameter) and thermocouple are flush mounted, while the absolute pressure sensor is 2 mm beneath the surface through a 1mm bore.

The measurement station are located as follows:

- pos. 1 : at the tank
- pos. 2 : 250 mm downstream of the tank
- pos. 3 : 318 mm upstream of the FOV
- pos. 4 : 160 mm downstream of the FOV
- pos. 5 : 1990 mm downstream of the FOV (10 mm from the dead-end)
- pos.6 : at the end (only dynamic pressure)

For the 19 mm test element, stations 5 and 6 are replaced by one single measurement module with a screw adapter to the pipe (weld-on *Swagelok* type) as depicted in Fig.5. The inner diameter of the adapter has been re-worked so that a constant inner diameter without step (that might cause turbulence and induce flow perturbation) is obtained.

As an additional sensor, an accelerometer is placed at the dead-end in order to measure structural vibrations. However results of this measurement are beyond the scope of the present paper and therefore not discussed here.

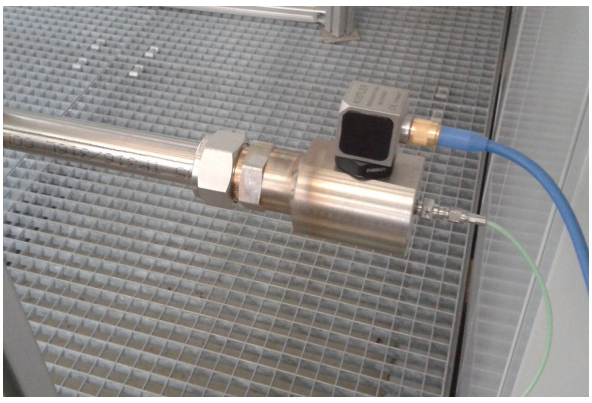

Figure 5: Screw connection of the measurement module at the dead-end. The sensor on top of the module (blue cable) is an accelerometer used for vibration measurements

## 3.2 Test Procedure

Before each test the downstream line is purged with gaseous nitrogen (GN2) flow by opening MV-4 and MV-2 and unscrewing the measurement module at the test-element end. After this operation, the test-section is evacuated by means of a vacuum pump (MV-3 open) to the desired vacuum level. The fast opening valve FOV and MV-2 are then closed and the MV-1 is opened to manually prime the upstream pipe. At this point, automatic operations are performed by the controlling software: tank pressure is set at a given value, FOV opens and data are recorded for 4 seconds.

## 3.3 Test-matrix

First, tests with GN2 at ambient pressure in the test-element are performed, rising the tank pressure progressively from 10 bar until the maximum design pressure of the test-element is reached (200 bar). Then, the tank pressure is set at 20 bar and the downstream line is evacuated at different vacuum pressure levels, namely 300, 100, 20 mbar. Tests are repeated 3 times for each test conditions to examine reproducibility

# 4 TEST RESULTS

The experimental investigation includes priming test in both a pre-pressurized and an evacuated pipeline. For all the tests, the fast acting valve opens at 700 ms; the water hammer phenomenon takes place and it is completely damped in 500-700 ms, depending on the operating conditions.

### Preliminary test

In the qualification campaign, two questions are addressed. In all the previous mentioned studies, only diameters of 6.35 mm (1/4") up to 12.7 mm (1/2") have been used and no data are available for bigger diameter as the one used in the present work. With such a relative large 22 mm diameter, flow stratification may occurs with eventually a correlated pressure difference. Thanks to the large diameter, it has been possible to install two dynamic pressure sensors at the dead-end, one at the bottom and one at top position, both facing the liquid front. Fig 6 shows the sensors arrangement at the dead-end for the 22 mm pipe.

After several experiments with both vacuum and ambient pressure downstream no difference at all was measured. To be sure that the sensors offset is not compensating any possible difference, the dead-end measurement module has been turned 180° and again no difference was measured.

The second question was to see if the pressure values at 10 mm from the end are different compared to the one at the end position. In a previous work conducted by Lema [6] with a similar arrangement the pressure difference between the two positions (20 mm) was quite remarkable. However, all the test run showed no difference at all in the pressure signal between the sensor at the dead-end (facing the fluid) and the one 10mm upstream (flush mounted, perpendicular to the flow direction).

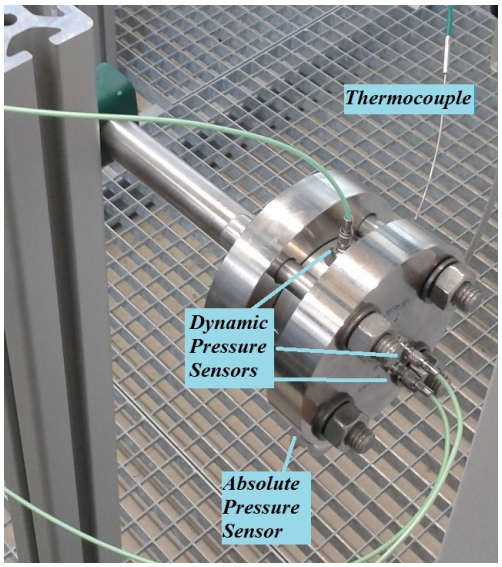


Figure 6: Sensor arrangement at the dead-end flange of the test-element: 3 dynamic pressure sensors (green cables), thermocouple and absolute pressure sensor (at the bottom, not visible)

## 4.1 Pre-pressurized line case

Test in pre-pressurized line for different tank pressures are shown in Fig. 7

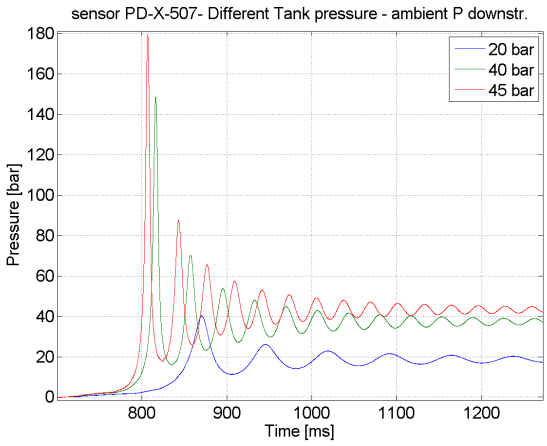


Figure 7: Test in pre-pressurized line for different tank pressures

As an interesting fact, a first pressure perturbation at the dead-end occurs after 6 ms, then a small step-plateau profile is repeated for another short time-span of about 40ms (Fig.8). These perturbations are the shock waves in the gas. In fact the perturbation travels at the speed of sound, which for nitrogen at ambient temperature is 346 m/s. For the given 2000 long test-element the travel time to reach the end of the first perturbation is then calculated in 5.8 ms. Afterward, the liquid front flowing in the pipe makes shorter and shorter the traverse length of the gas, thus reducing the travel time of the shock wave.

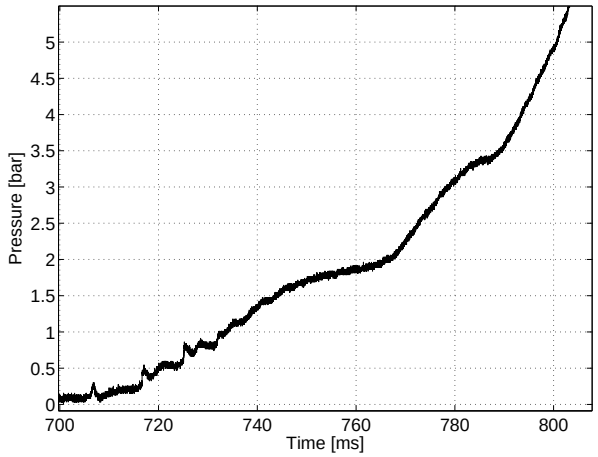


Figure 8: Detail of the shock-wave induced pressure perturbations

## 4.2 Evacuated line case

Fig.9 shows the pressure evolution for three different vacuum levels tested, namely 300, 100 and 20 mbar.

As expected, pressure peaks increase with decreasing line pressure level, and the frequency of the oscillations also increases.

After the first peak no cavitation is achieved although the pressure peak is 200 bar. This is due to the amount of residual gas and/or the dissolved gas in the liquid that prevents column separation from taking place. Future tests will be performed at higher vacuum level (<10 mbar), considering that for line pressures below the saturation pressure of water (20 mbar) the liquid front will undergo flash boiling.

Fig. 10 shows the evolution of the first pressure peak. The profile has a multiple step rise, each followed by a very fast plateau of 0.1 ms. This curios pressure rise has already been notice in previous experiments performed by Lecourt and Steelant [7]. The authors postulated that this multiple step increase is related to two-phase flow phenomena.

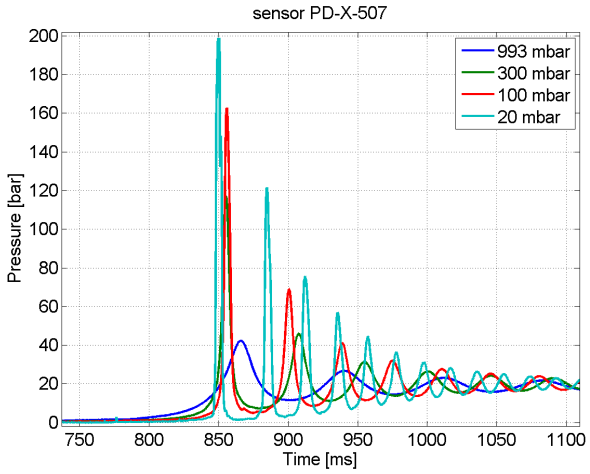


Figure 9: Priming test for different vacuum levels

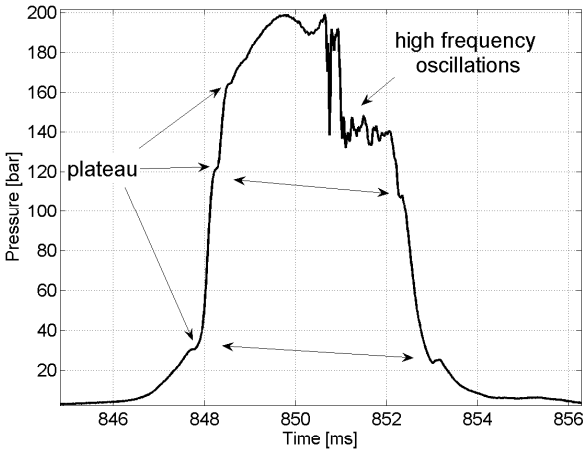


Figure 10: Detail of the evolution of the first pressure peak for priming test in vacuum

At the highest pressure value, between 850-852 ms, an unexplained pressure drop from 200 to 140 bar takes place. This could be due to the gas bubble collapsing that creates an additional volume for the liquid causing an expansion and therefore a pressure drop. This negative pressure gradient seems too severe to be caused by fluid-structure interaction. It is followed by high frequency oscillations that might be au contraire due to structural interaction rather than fluid-dynamics effects. Visual investigations by means of a transparent pipe will help to gain an insight in this complex transient. To this purpose an upgrade of the measurement technique is in progress.

Also interesting, the down-slope presents a symmetrical step profile with two plateaux almost at the same pressure level as the up-slope. This symmetry of the plateaux may confirm that the step increase (and decrease) profile is due to two-phase flow phenomena such as absorption (desorption) of the residual non condensable gas in the line.

| *Tank pressure [bar]* | *Line pressure [mbar]* | *Pressure peak [bar]* | | | | | *Peak time [ms]* | | |
|---|---|---|---|---|---|---|---|---|---|
| | | ***Exp*** | *Predicted* | | | | ***Exp*** | *Predicted* | |
| | | | *adiab.* $\gamma = 1.4$ | *isoth.* $\gamma = 1$ | *polytr.* $\gamma = 1.3$ | *Ecosim* | | *polytr.* $\gamma = 1.3$ | *Ecosim* |
| 20.31 | 993 | **42.58** | 40.9 (-4%) | 51.2 (17%) | 43.7 (-0.1%) | 51.3 (17%) | **164.5** | 153.9 | 153.4 |
| 20.30 | 993 | **42.29** | | | | | **166.1** | | |
| 20.32 | 993 | **46.37** | | | | | **162.0** | | |
| 39.48 | 990 | **148.6** | 115.6 (-21%) | 199.0 (42%) | 137.5 (-5%) | 178.5 (23%) | **116.3** | 106.1 | 104.7 |
| 39.51 | 992 | **149.9** | | | | | **114.8** | | |
| 39.50 | 992 | **138.2** | | | | | **116.8** | | |
| 42.56 | 993 | **164.3** | 131.2 (-20%) | 252.2 (54%) | 154.4 (-6%) | 198.1 (21%) | **110.7** | 102.6 | 100.7 |
| 45.10 | 993 | **187.3** | 144.8 (-19%) | 296.3 (64%) | 171.8 (-4%) | 214.0 (19%) | **106.6** | 99.4 | 97.7 |
| 45.10 | 993 | **175.0** | | | | | **107.6** | | |
| 45.14 | 994 | **179.5** | | | | | **106.9** | | |
| *Vacuum case* | | | | | | | | | |
| 20.16 | 21 | **198.9** | 201.3 (<0.1%) | | | 201.8 (0.3%) | **150.6** | 140.5 | 137.4 |
| 20.17 | 22 | **203.7** | | | | | **153.0** | | |
| 20.14 | 20 | **201.0** | | | | | **151.4** | | |

Table 1: Summary of analysis with experimental data. Error difference is calculated with the average value of the experimental results

From an experimental point of view, reproducibility at vacuum condition is much better than the ambient case. For the 20 mbar pressure in the downstream line, the measured pressure peak difference among the three tests is less than 1.5%.

### 4.3 Analytical results vs test data

Table 1 summarizes the test results of the analytical model in comparison with the experimental data. The experimental pressure peaks fall between the prediction of adiabatic compression and isothermal compression. Adiabatic compression is better in terms of error accuracy, but always underestimated, while isothermal compression is always overestimated. The polytropic compression with polytropic index $\gamma = 1.3$ gives very accurate predictions (error <6%) and it is therefore recommended to be used. The numerical impact time is always occurring before the experimental one. For the vacuum case, the numerical results are very accurate, although tested only at one test condition of 20 bar tank pressure.

The prediction ability with the rigid liquid column model are satisfactory, especially with the assumption of polytropic compression with index $\gamma = 1.3$ predictions are very close to the experimental values.

## 5 NUMERICAL SIMULATION WITH ECOSIMPRO/ESPSS

A numerical model of the test-bench is built by using software EcosimPro® in conjunction with ESPSS library, an ESA-developed tool capable of one dimensional, two-phase flow transient simulations. The model schematics used for the simulation is shown in Fig. 11

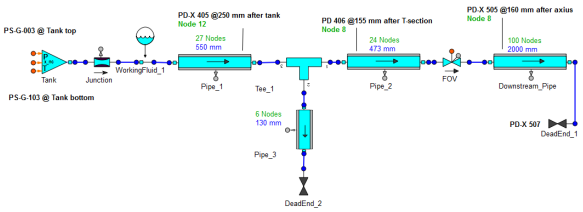


Figure 11: EcosimPro model of the test-bench used for the simulation. The 2000 mm test element is modeled with 100 nodes.

Two test-cases are simulated: a) ambient pressure in the line; b) vacuum condition 20mbar in the line. Tank pressure in both cases is 20 bar.

The first simulation run without any correction factor overpredicts the pressure peak by far, for both ambient and vacuum scenario. This is not caused by the number of nodes, as the choice of 100 nodes is done on the basis of a grid sensitivity study (initially only 25 nodes were chosen, then increased until convergence was considered acceptable at 100 nodes).

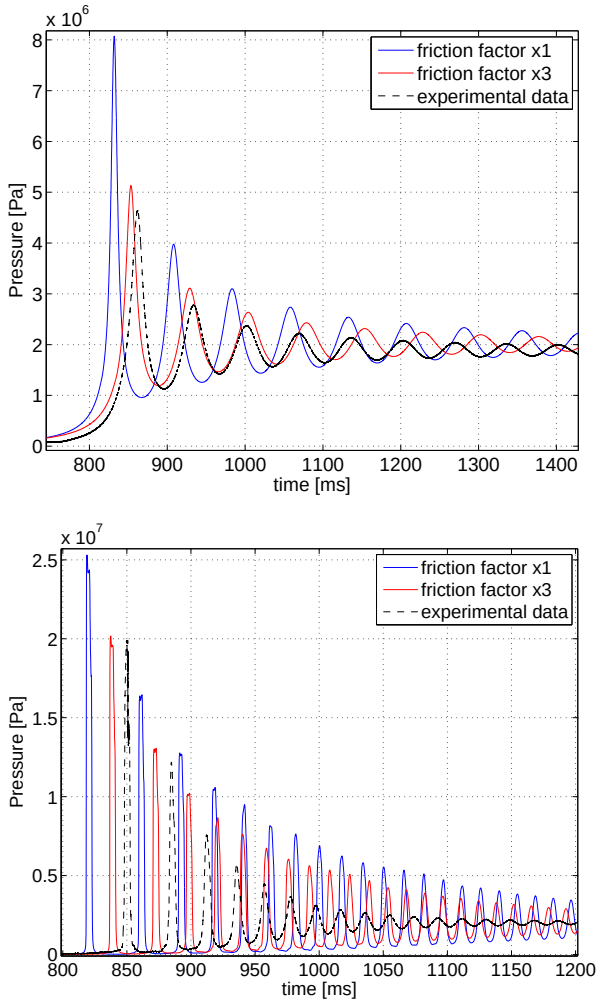


Figure 12: Comparison between numerical results and test data. Top: ambient pressure gas in the test-element; bottom: vacuum case (20 mbar in the test-element)

It has been decided then to increase the friction factor to adjust the pressure peak. The increase of the friction factor is physically motivated by the unsteady conditions of the flow. Changes occurring in the velocity profile during acceleration of the flow produce varying shear stress at the wall. Due to this varying shear stress, the viscous boundary layer is not established and a higher velocity gradient is found at the wall than would be expected for steady flow. Because of the higher velocity gradient at the wall, a greater friction coefficient shall be used. Empirically a multiplier value of 3 has been found to agree better with the data. In both cases, while the pressure peak is artificially adjusted, the impact time is faster than the experimental data. Frequency is also in good agreement, whereas the damping of the pressure signal is under-estimated by far, being the experimental data faster attenuated (Fig.12). The reason is the difficulty in modeling two-phase flow aspects such as cavitation, condensation and eventually also absorption/desorption of a non condensable gas in the liquid. The damping in the ambient scenario is in fact better predicted.

For the vacuum scenario, the minimum pressure after the first pressure peak is 18 KPa, still not low enough to achieve cavitation, while the experimental value is 110 KPa. The difference is likely due to the mixing of the liquid with the residual gas in the line that is not properly modeled.

Future simulations will address more in details the effect of the numerical damping and the effect of the dissolved gas in the liquid, as it affects the speed of sound, and thus the pressure peak and the frequency.

# 6 CONCLUSIONS

At DLR Lampoldshausen a new test facility to investigate fluid transient phenomena has been built and in detail described. Purpose of this new test facility is to reproduce the water hammer and priming processes occurring in spacecraft and satellite feed-lines during the start-up transient. Unlike previous similar experiments, a relative large diameter (19.05 mm) for the test-element has been used in order to examine high mass flow that are typical of spacecraft feedlines like the ESA automatic transfer vehicle ATV.

Several priming test in both pre-pressurized and evacuated pipeline have been performed and results compared against numerical simulation.

The experiments in vacuum condition showed an interesting pressure evolution with multiple step-plateau. A symmetry of this profile between the up-slope and the down-slope of the first pressure peak has been observed. A possible interpretation of this profile has been provided.

The analysis with the rigid liquid column theory gives satisfactory results and it has been demonstrated that the assumption of polytropic compression with index $\gamma = 1.3$ provides very accurate predictions close to the experimental values. In addition, numerical simulations have been run by using EcosimPro® software in conjunction with ESPSS library. Results indicated that the friction value must be increased up to 3 times in order to take into account the unsteady flow conditions. Compared to the experimental values, EcosimPro numerical results are not in well agreement, in particular the damping of the pressure wave in vacuum condition is under estimated by far. The reason is the lack of accurate models that properly consider two-phase flow aspects such as cavitation, condensation and eventually also absorption/desorption of a non condensable gas in the liquid.

Future experiments shall focus on the fluid-structure interaction. In particular the influence of the pipe connection (flange, welding, screw) on the pressure peak needs further investigations.

# References


[1] Michael J. Morgan. Pressure transient characterization test for star-2 propulsion system fuel manifold. In *40th AIAA/ASME/SAE/ASEE Joint Propulsion Conference and Exhibit*, 2004.

[2] Henry C Hearn. Development and application of a priming surge analysis methodology. In *41st AIAA/ASME/SAE/ASEE Joint Propulsion Conference & Exhibit*, 2005.

[3] A.R. Scroggins. A streamlined approach to venturi sizing. In *41st AIAA/ASME/SAE/ASEE Joint Propulsion Conference & Exhibit*, volume 2012-4028, 2012.

[4] Chang Yeol Joh and Kum Dang Park. Pressure surge analysis and reduction in the kompsat propellant feed system. In *Proceedings KORUS 2000. The 4th Korea-Russia International Symposium on Science and Technology*, 2000.

[5] I. Gibek and Y. Maisonneuve. Water hammer tests with real propellants. *AIAA*, 4081, 2005.

[6] M.Lema and J.Steelant. Experimental characterization of the priming phase using a propellant line mock-up. *Space Propulsion Conference, Bordeaux, France*, May, 8 2012.

[7] Renaud Lecourt and Johan Steelant. Experimental investigation of waterhammer in simplified feed lines of satellite propulsion systems. *Journal of Propulsion and Power*, 23:1214–1224, 2007.

[8] K.L. Yaggy. Analysis of propellant flow into evacuated and pressurized lines. *AIAA*, (1984-1346), June, 11 1984.

[9] R.P. Prickett, E. Mayer, and J. Hermel. Water hammer in a spacecraft propellant feed system. *Journal of Propulsion and Power*, 8:592–597, 1992.

[10] T.Y. Lin and D. Baker. Analysis and testing of propellant feed system priming process. *Journal of Propulsion and Power*, 11:505–512, 1995.